Carpathian Journal of Earth and Environmental Sciences, February 2020, Vol. 15, No. 1, p. 197 - 210; Doi:10.26471/cjees/2020/015/122

# USEFULNESS OF SENTINEL-2 VISIBLE LIGHT SATELLITE PHOTOS FOR SURVEYS OF HYDRODYNAMIC PHENOMENA IN POLISH CARPATHIAN STORAGE RESERVOIRS

**Paweł S. HACHAJ[1] & Katarzyna KOŁODZIEJCZYK[1]**

*[1]Faculty of Environmental and Power Engineering, Cracow University of Technology, Warszawska 24, 31-155 Cracow, Poland, e-mail: pawel.hachaj@iigw.pk.edu.pl, katarzyna.kolodziejczyk2@pk.edu.pl*

**Abstract:** The aim of the research presented in this paper was the recognition of potentials and drawbacks of visible light photos taken by the Sentinel-2 satellites as a source of data for hydrodynamic issues regarding dammed reservoirs located in the Polish Carpathian foothills. The authors analyzed the photos of five reservoirs: Goczałkowice, Tresna, Dobczyce, Czorsztyn and Solina. Depending on the object's geographic location, one can expect one or two photos taken during each 5-day period. No more than 1/5 of the taken photos of the given locations contain a non-obscured view of the water bodies. Visibility varies throughout the year along with the expected clear sky percentage; and the probability of obtaining a clear picture is lower than this value. In the Polish Carpathians, the best visibility occurs in August, while the worst in December. The chance of getting a clear view is lower during high discharge periods than in low discharge ones. In the clear photos the authors identified density currents of different nature: turbidity, reverse turbidity (i.e. clear water entering a turbid area), eutrophic and thermal. The currents can also be seen as sub-glacial ones. The shapes of the visible currents can be used for calibration and validation of hydrodynamic numerical models of the reservoirs. The authors obtained a good accordance between the shapes of the currents visible on the photos and the water velocity field predicted by a numerical simulation with the FESWMS model for the hydrological and meteorological input variables set to follow the actual conditions that day.

**Keywords:** Sentinel-2, satellite images, storage reservoir, turbidity current, density current, sub-glacial flow

## 1. INTRODUCTION

Dammed storage reservoirs are important elements of the local and regional river system. They are established by building a dam at a given river cross-section and they are designed to play one or more of the following functions: flood and drought protection, energy production, industrial and drinking water supply, recreation, aquatic life habitats and refuges, and more. As such, their quality state and ecological potential are subjects of interest for water management. Therefore, every potential source of data about them is worth considering from the water management related research projects.

The Sentinel-2 satellite missions (Gatti & Bertolini, 2015; Gatti & Galoppo, 2018) are aimed towards multi-scope and multi-purpose monitoring of the Earth surface. This includes collecting data about vegetation, soils, inland and coastal waters etc. Sentinel-generated data were the base for numerous recent scientific papers concerning for example: lake overgrowing (Robak et al., 2016), lake water quality issues (Liu et al., 2017; Karaoui et al., 2019), landslide monitoring (Lacroix et al., 2018), tree species identification (Karasiak et al., 2017), water demand assessment (Vanino et al., 2018). In all those cases the satellite monitoring was an enhancement or even a replacement of traditional onsite measurements. Traditional means are expensive and time consuming as well as spatially limited (Silva et al., 2008; Sojka, 2019). While satellites are very expensive on their own, once they are on their orbits, they can generate extensive amount of spatially broad data at a small cost per obtained data unit. High resolution of the Sentinel-2 satellite photos (10 meters per pixel) along with frequent recurrence of the data (currently the Sentinel-2 satellites take a photo of a given place at least once every five days) make them a good material for comparative studies (Sojka et al., 2019).

The Remote Sensing of Environment journal devoted a special issue (Vol. 157, 2015) solely to the remote sensing of inland waters (Palmer, 2015). Another special issue of this journal (Vol. 225, 2019) focuses on scientific and applied usage of the Sentinel satellite images. According to Dörnhöfer & Oppelt (2016) Web of Knowledge query, the number of scientific papers containing phrases "<lake|inland> water <quality|ecology>" and "remote sensing" was continuously growing during the years 2000-2014. This is the effect of the increasing amount and accessibility of the appropriate data. Currently the daily download of the Sentinel-2 data exceeds 7 TB.

The aim of the research presented in this paper was the recognition of the potentials and drawbacks of visible light photos taken by the Sentinel-2 satellites as a source of data for hydrodynamic issues regarding dammed reservoirs located in the Polish Carpathian foothills.

## 2. MATERIALS AND METHODS

### 2.1. Study sites

The objects chosen for the study are five big dammed reservoirs located in the upper Vistula catchment: Goczałkowice, Tresna, Dobczyce, Czorsztyn and Solina.

The last four are strictly Carpathian reservoirs, the first one is located outside the Carpathians, but over ¾ of its catchment lies within this region. They are depicted on the map (Fig. 1) along with the ranges of the upper Vistula catchment and the Polish Carpathians; their characteristics have been summarized in Table 1.

A brief description of the reservoirs follows:

• **Czorsztyn**: It is the first and the biggest (in terms of capacity) reservoir of the Dunajec river cascade; the other reservoirs on the Dunajec are: Sromowce, Rożnów and Czchów. It is a multi-purpose reservoir used for flood and drought protection, energy production and recreation (Jaguś & Rzętała, 2010; Jokiel et al., 2017). As it is a mountainous reservoir, the weather in its surroundings tends to change frequently and rapidly (Woś, 1996; Jaguś & Rzętała, 2010).

• **Dobczyce**: The primary function of this reservoir is supplying water for the city of Kraków. It serves as the main source of drinking water for the city. As such, it is closed for recreation. Its secondary functions are flood and drought protection and energy production, (Hennig, 1991; Jokiel et al., 2017). This reservoir is among top priority objects of concern for the authors' home Department.

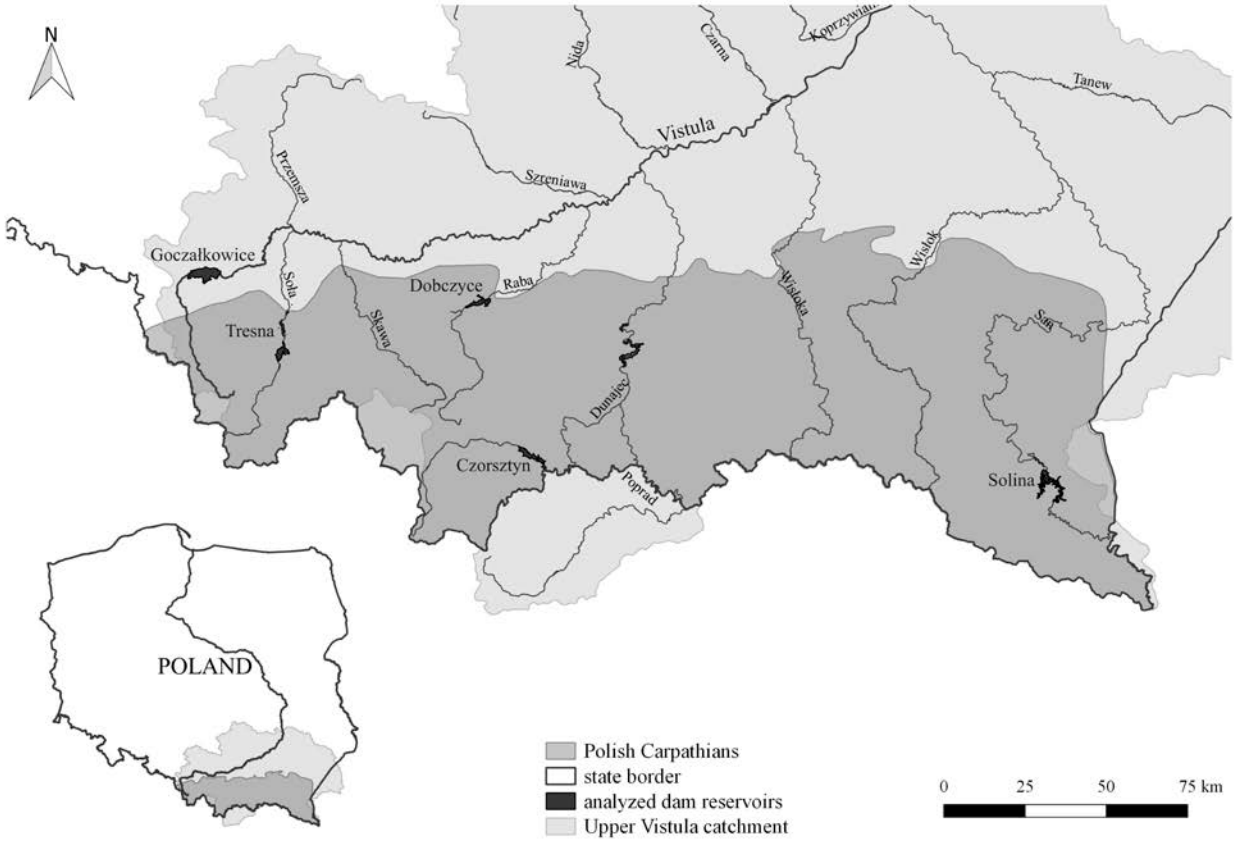


Figure 1. Study area location.

Table 1. Dam reservoirs characteristics (based on: Hennig, 1991; Hachaj, 2007; Bielak, 2009, Augustyn, 2010; Jaguś & Rzętała, 2010; Bartoszek & Czech, 2014; Jachniak & Suchanek, 2015; Neverova-Dziopak & Droździk, 2017; GUS 2017; Jokiel et al., 2017).

| Reservoir | Czorsztyn | Dobczyce | Goczałkowice | Solina | Tresna |
|---|---|---|---|---|---|
| River | Dunajec | Raba | Mała Wisła | San | Soła |
| Coordinates | N 49°26' | N 49°52' | N 49°56' | N 49°23' | N 49°43' |
| | E 20°18' | E 20°05' | E 19°55' | E 22°27' | E 19°12' |
| Section of river [km] | 173.3 | 60.1 | 42.8 | 325.2 | 40.0 |
| Area at maximum accumulation [km$^2$] | 11.00 | 10.11 | 32.00 | 22.00 | 9.64 |
| Total capacity at maximum accumulation [mln m$^3$] | 231.9 | 137.9 | 166.7 | 472.0 | 96.1 |
| Damming height [m] | 56.0 | 30.5 | 14.0 | 57.5 | 23.0 |
| Average depth [m] | 11.0 | 10.2 | 5.5 | 22.0 | 9.4 |
| Max depth [m] | 49.5 | 28.0 | 13.0 | 60.0 | 28.0 |
| Average water surface level [m a.s.l.] | 520 | 268 | 257 | 420 | 343 |
| Catchment area [km$^2$] | 1147.0 | 768.0 | 523.0 | 1189.0 | 1037.0 |

• **Goczałkowice**: It is a multi-purpose reservoir. It serves for flood and drought protection; it is a water source for the Silesian agglomeration and there are "Natura 2000" bird protection areas there. Limited sailing is permitted on its waters (Bogdał et al., 2015; Jokiel et al., 2017).

• **Solina**: It is the deepest reservoir in Poland and one with the highest capacity (Koszelnik, 2013; Bartoszek & Czech, 2014). It is a mountainous reservoir and its catchment is in ¾ covered by forests (Bartoszek & Czech, 2014). Its tasks are energy generation, recreation as well as flood and drought protection (Hennig, 1991; Majewski, 2013; Jokiel et al., 2017).

• **Tresna**: The biggest reservoir of the Soła river cascade (the other reservoirs are Porąbka and Czaniec). Similarly, to most other reservoirs in the region, it is multi-purpose and is used for recreation, energy generation and flood and drought protection. (Jokiel et al., 2017).

### 2.2. Data collection and processing

Sentinel is a set of space missions performed by the European Space Agency (ESA,2019). It is a part of the European Union Copernicus program (Copernicus, 2019). There are six missions planned in total, named Sentinel-1 to Sentinel-6. The Sentinel-2 mission involves a pair of two identical satellites, Sentinel-2A (operational since June 2015) and Sentinel-2B (operational since March 2017) (ESA,2019). Both satellites are on sun-synchronized orbit. They take their photos at 10:30 local solar time. With two satellites, the revisit time is 5 days; due to overlapping some areas may be photographed more frequently. Both satellites are equipped with a high resolution multi-spectral instrument (MSI) that registers data with 13 spectral channels in the visible, near infrared, and short wave infrared spectral range. The width of the path on the Earth surface covered by those instruments is 290 km. In the visible range, there are 3 bands present: 492 nm (blue), 559 nm (green), and 665 nm (red), each of them with 10 m spatial resolution. There is a 478 ms offset between taking a photo in red and green bands and another 527 ms offset between green and blue ones, so for objects moving slower than 10 m/s all three colors overlap properly. (Gatti & Bertolini, 2015; Lavrova et al., 2016; Robak et al., 2016; Gatti & Galoppo, 2018; Rapinel et al., 2019; Sojka et al., 2019; MSI Instrument – Sentinel-2 MSI Technical Guide – Sentinel Online, 2019).

The Copernicus program offers free access to the image data generated by the Sentinel missions. The authors used the EO Browser (2019) to access and download the data. In principle, there are two types of visible light images provided, named L1C and L2A. The L1C version is the original RGB image as caught by the satellite sensors. The L2A is digitally filtered to reduce the bluish coloration and other optical effects caused by the atmosphere. While L2A photos look more natural and sharper than L1C, they actually do not contain more information than the other. Both versions of the same photo of the Dobczyce reservoir taken on 2017.05.28 are shown in Fig. 2 (A and C).

At the current stage, the authors focused primarily on visual identification of hydrodynamic phenomena that occur in storage reservoirs. Therefore, the images have been processed to

increase contrast of water areas. For the reservoirs, marquees (masks) have been defined to cover the flooded areas. Within these marquees, the global contrast has been increased linearly without clipping and/or disturbing the color balance. Outside the marquees, the images have been turned into grayscale by making each channel luminosity equal to the average value of the RGB channels for each pixel. Processed images are presented to the right of their unprocessed counterparts in Fig. 2 (B and D).

### 2.3. The FESWMS model

Observational data have been compared with the FESWMS model (Froehlich, 2003; Hachaj et al., 2014) outcome. FESWMS is a depth averaged flow model that simulates movement of water in rivers, estuaries, storage reservoirs, and coastal waters. FESWMS applies the finite element weighted residuals method to solve systems of equations that describe two-dimensional depth averaged surface water flow. It can be used to simulate flows in surface-water bodies where vertical velocities and accelerations are small in comparison to those in horizontal directions. It can simulate both steady and time-dependent surface water flows.

Equations describing depth-averaged surface-water flow are found by integrating the three-dimensional mass and momentum transport equations with respect to the vertical coordinate. The vertically integrated continuity equation is:

$$\frac{\partial z_w}{\partial t} + \frac{\partial q_1}{\partial x} + \frac{\partial q_2}{\partial y} - q_m = 0 \qquad (1)$$

where: $z_w$ – water surface elevation, $q_1$ – unit flow rate in the horizontal $x$ direction, $q_2$ – unit flow rate in the horizontal $y$ direction, $q_m$ – total inflow/outflow rate per unit area.

The equation describing momentum transport in the $x$ direction is as follows:

$$\frac{\partial q_1}{\partial t} + \frac{\partial}{\partial x}\left(\beta \frac{q_1^2}{H} + \frac{gH^2}{2}\right) + \frac{\partial}{\partial y}\left(\frac{\beta q_1 q_2}{H}\right) + \frac{1}{\rho}\left(\tau_{bx} - \tau_{sx} - \frac{\partial(H\tau_{xx})}{\partial x} - \frac{\partial(H\tau_{xy})}{\partial y}\right) + gH\frac{\partial z_b}{\partial x} - \Omega q_2 = 0 \qquad (2)$$

where: β – momentum flux correction coefficient that accounts for the variation of velocity in the vertical direction, $H$ – water depth, $z_b$ – bed elevation, g – gravitational acceleration, ρ – water density (considered constant), $\tau_{bx}$, $\tau_{by}$ – bed shear stresses acting in the $x$ and $y$ directions, $\tau_{sx}$, $\tau_{sy}$ – surface shear stresses acting in the $x$ and $y$ directions (usually caused by the wind), $\tau_{xx}$, $\tau_{xy}$ – internal shear stresses caused by turbulence, Ω – Coriolis parameter.

The equation describing momentum transport in the $y$ direction is fully symmetrical to the above.

## 3. RESULTS AND DISCUSSION

### 3.1. General visibility of the reservoirs

Currently, when two Sentinel-2 satellites are on their orbit, in the Upper Vistula catchment one can expect a pair of L2A and L1C images of a given area to be taken either once or twice every five-day period. In the majority of the catchment area, photos are taken twice, with a pattern “PnPnn” where P denotes

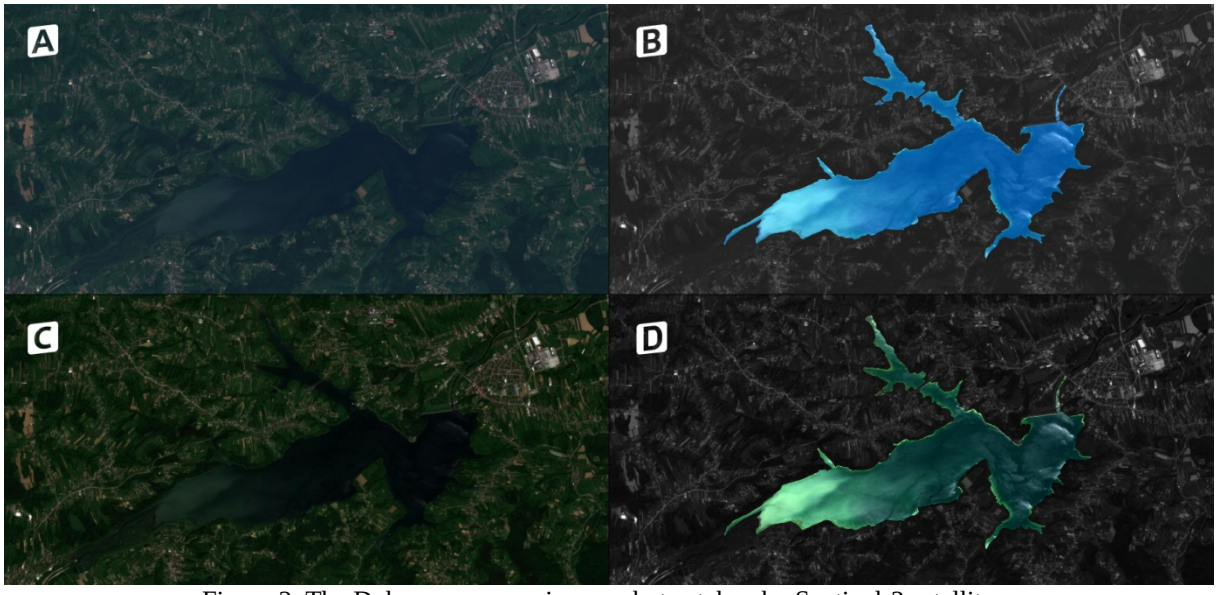


Figure 2. The Dobczyce reservoir area photos taken by Sentinel-2 satellites:
A: "L1C" photo: B: processed image "L1C"; C: "L2A" photo; D: processed image "L2A"

a day with photos taken and n denotes a day with no photo taken. Occasional malfunctions may cause a photo not to appear on a day it is expected, but they do not disturb the pattern; they just replace a single "P" with an "n" within the sequence. Such malfunctions may concern both L2A and L1C images or only one of them; in the latter case there is still one image available in the given day.

The satellites photograph the Earth below with no regard to the visibility conditions in the photographed area. Obscuring the view by a cloud cover has been mentioned as a common nuisance in several papers regarding the use of the Sentinel data for aquatic objects, e.g. (González-Jorge et al., 2018; Condé et al., 2019; Pahlevan et al., 2019). This factor is highly sensitive to the geographical location of the object in question; while (Karaoui et al., 2019) seemingly have no problems with clouds when working with satellite images of a storage reservoir located in Morocco, any study regarding dammed reservoirs in central Europe should take this issue into account.

For the purpose of this paper the authors reviewed all the Sentinel-2 photos of the five Polish reservoirs described in the previous section (Czorsztyn, Dobczyce, Goczałkowice, Solina, and Tresna) from the beginning of the Sentinel-2 mission (June 2015) until the end of May 2019. The photos have been classified into five categories with respect to the visibility of the reservoir:

A. **Clear view.** No clouds or mist/fog obscure the reservoir surface. The details are visible, the image contrast and saturation are good. Such photos may be analyzed automatically or manually.

B. **Unclear view.** Small clouds may partially cover minor areas within the given reservoir and/or the weather may be misty, and as such decrease the contrast and saturation of the whole image or some of its parts. Manual analysis is feasible. Automatic analysis is possible with caution, as the algorithms may give misleading results.

C. **Obscured view.** Big parts of the reservoir in question are cloud-covered. Some phenomena may be detected and recognized, but the image does not qualify for any systematic analysis, especially an automatic one.

D. **Invisible.** The reservoir is totally covered and none of its features is visible.

E. **Corrupt.** The image exists in the data base, but it does not show the object.

The results are presented in Tab. 2 and Fig. 3.

Table 2. Visibility of five Polish storage reservoirs in the Sentinel-2 photos (June 2015 – May 2019).

| Reservoir | A (clear view) | B (unclear view) | C (obscured view) | D (invisible) | E (corrupt) |
|---|---|---|---|---|---|
| Czorsztyn | 19.7% | 9.2% | 15.2% | 55.7% | 0.2% |
| Dobczyce | 18.7% | 13.5% | 11.6% | 56.2% | 0.0% |
| Goczałkowice | 8.1% | 6.4% | 5.7% | 29.5% | 50.4% |
| *Goczałkowice | 16.3% | 12.9% | 11.5% | 59.5% | 0.0% |
| Solina | 20.4% | 11.3% | 11.8% | 56.3% | 0.2% |
| Tresna | 18.8% | 8.3% | 12.6% | 60.2% | 0.0% |

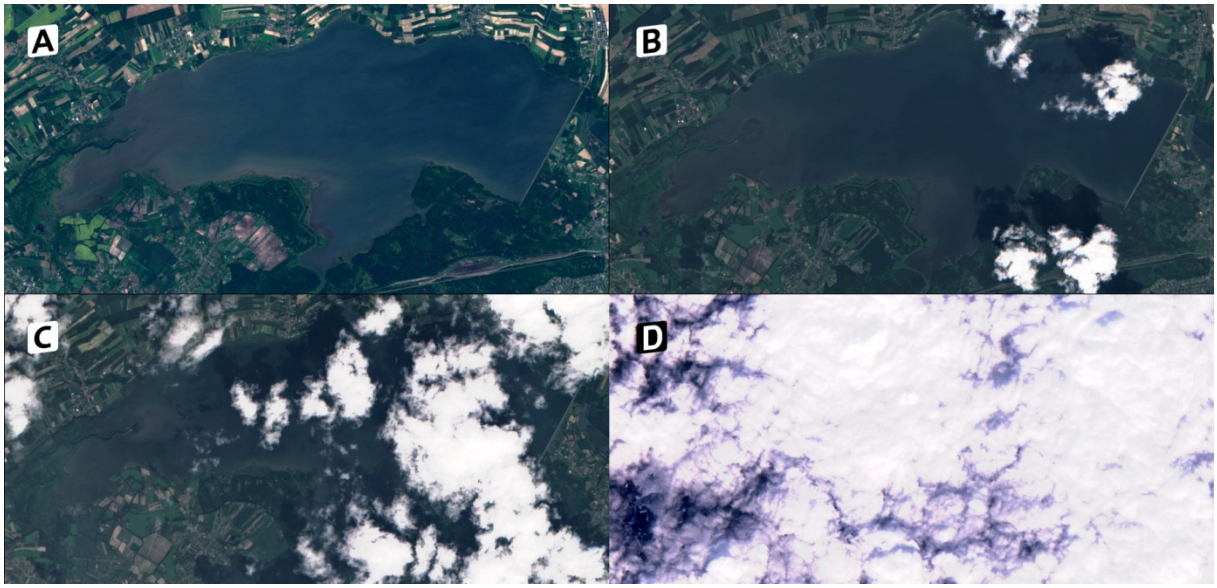


Figure 3. The Goczałkowice reservoir area photos of "L1C" type taken by Sentinel-2 satellites: A: clear view: B: Unclear view; C: Obscured view; D: Invisible.

The high percentage E-rated photos of the Goczałkowice reservoir is a consequence of its geographical location: about every other photo of this area has the reservoir on its edge. As a result, only the easternmost part of the reservoir appears on those photos. This is the consequence of the way that the Sentinel-2 satellites collect their data, as described above, not an error; a picture containing the whole reservoir is taken once every five days. The star-marked row of the Tab. 2 presents the visibility of the Goczałkowice reservoir taking into account only the photos with the whole object present in a photo. For the other reservoirs, the fraction of E-rated photos is close to zero.

For non-corrupt photos one can expect 16-21% of clear reservoir images and 27-33% of images that are at least satisfactory (categories A and B combined).

It should be noted that the fraction of satisfactory images can be lower than expected if one takes into account the average fractions of sunny and cloudy days in a given region. Water bodies can generate local clouds of fog. Such situations are shown in Fig. 4. Fig 4A presents the area of the Czorsztyn reservoir. The sky is clear all around, but a thick cloud of fog lies over the water surface, which qualifies the image into the "D" category. (The bright crescent in the upper part of the image is not an artifact: there is a ski resort there.) Fig 4B shows the Tresna reservoir with clouds of mists over the water surface (which qualifies the photo into the "C" category) while the surroundings of the reservoir are clear.

Table 3. Probabilities of getting a clear ("A"- rated) or good ("A" or "B"- rated) image of a reservoir in a given month and average percentage of clear sky in the same month.

| | "A"- rated photo percentage | "A"&"B"- rated photo percentage | Clear sky percentage |
|---|---|---|---|
| January | 14 | 19 | 15 |
| February | 20 | 25 | 18 |
| March | 15 | 25 | 26 |
| April | 20 | 39 | 37 |
| May | 20 | 34 | 33 |
| June | 12 | 33 | 32 |
| July | 13 | 28 | 33 |
| August | 34 | 46 | 35 |
| September | 30 | 43 | 38 |
| October | 26 | 30 | 30 |
| November | 16 | 20 | 18 |
| December | 11 | 14 | 15 |

Table 3 presents a monthly breakdown of visibility integrated for all 5 considered reservoirs for non-corrupt photos only. It shows that the highest chance of, getting A- or B-rated photo is in August while the lowest is in December. As expected, the chance of obtaining a good photo in a given month is well correlated with the average clear sky percentage during that month: the correlation coefficient between the average clear sky percentage and the chance of getting "A" or "B" rated photos in a given month is 0.90, while 0.82 is required for the correlation significance level of 1‰. If only "A" rated photos are taken into account, the correlation between the chance of getting such a photo in a given month and the average percentage of clear sky during that month is 0.56, resulting in 6% of correlation significance level.

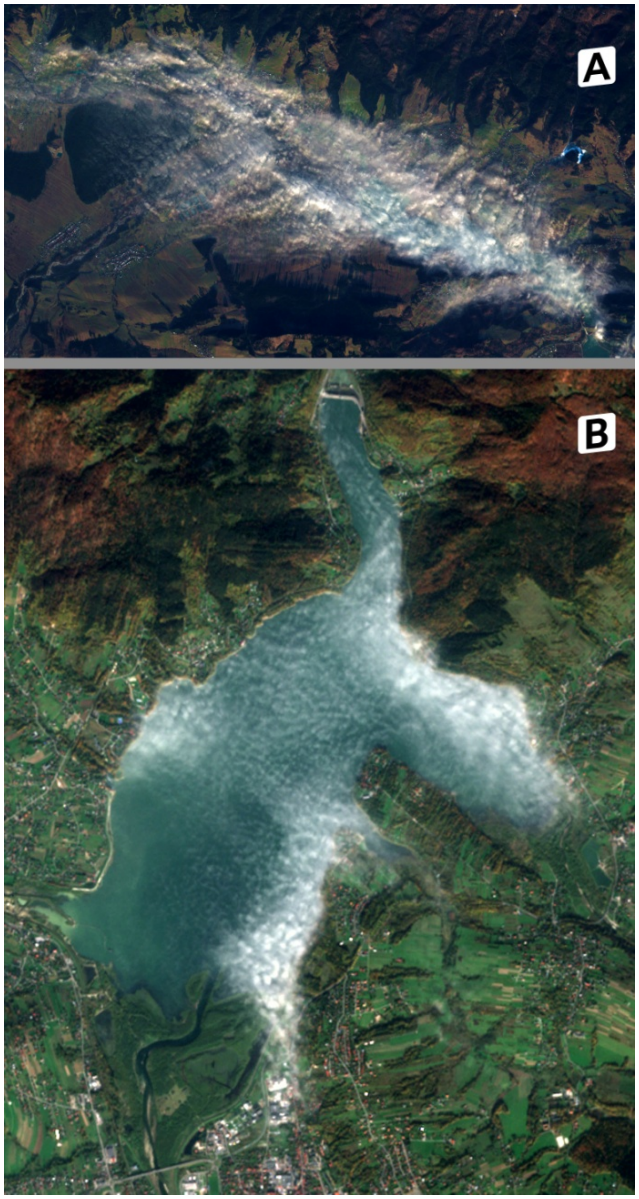


Figure 4. Czorsztyn (A) and Tresna (B) reservoirs view obscured by local mists.

### 3.2. Currents visibility

Mass transport in reservoirs is often accomplished by currents. Numerous studies have been performed on the so-called turbidity currents, when turbid water (a mixture of water and sediment) enters a clear water body like a reservoir, a lake, or an estuary, see e.g.: (De Cesare et al., 2001; Schleiss et al., 2009; Hu et al., 2015; He et al., 2018). Turbidity currents form a subset of a more general phenomenon of density currents (Thornton et al., 1996; Chen & Fang, 2015; Abbasi et al., 2016; Goleij et al., 2017). As the name suggests, the density of water within the current differs from the density of stagnant water around. This may be caused by particles suspended in water (like sediment for turbidity currents but also small life forms like phytoplankton), by different salinity or by different temperature of the water. It is noteworthy that the difference may be positive as well as negative – e.g. eutrophic water may form a density current in clear water and vice versa.

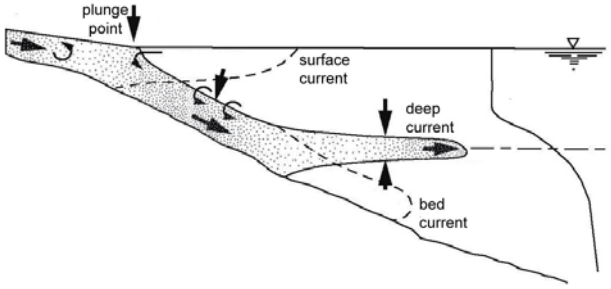


Figure 5. Types of currents in a flow-through lake or reservoir – vertical cross-section (Ford, 1990).

Lake and reservoir currents usually originate from one of the inflows of the water body in question. When reaching deeper parts of the reservoir, currents may remain on the surface or they may plunge (Savage & Brimberg, 1975; Akiyama & Stefan, 1984; Dai & Garcia, 2009; Cortés et al., 2014), and propagate further as deep or bed currents – see Figure 5.

In planar view, all the surface currents in storage reservoirs can be divided into four categories as shown in Figure 6. They are as follows:

A. Open currents. They start at the mouth of the main reservoir in flowing river and end in the main reservoir outflow. Usually there can be only one open current in a given reservoir (thus called the main current) or no open currents at all.

B. Half-open currents. They start at the mouths of significant reservoir inflows, then they either plunge or disperse. Less commonly, they may appear close to the reservoir outflow and lead to that outflow.

C. Loop currents. They form closed shapes that may resemble whirlpools; however, they are neither real nor potential whirls (or vortices) as those phenomena are understood in hydrodynamics, see (Williams et al., 2011). So, it is more appropriate to call them “loops” or “circulations” instead.

D. Fragmentary currents. They appear in a certain spot of the reservoir surface and disappear in another. They can be understood as parts of larger structures that have other parts submerged.

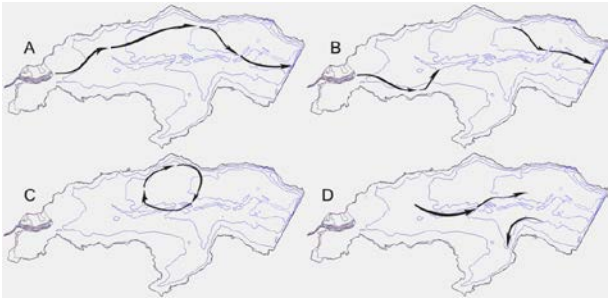


Figure 6. Types of surface currents In a flow-through Lake or reservoir – planer view:
A: open current; B: half-open currents; C: loop current; D: fragmentary currents (Hachaj, 2019).

Currents contribute to the evolution of a wide range of sedimentary structures and other morphological features in flow-through lakes and artificial reservoirs (De Cesare et al., 2001; Schleiss et al., 2009; Meiburg & Kneller, 2010). As such they are object of interest for many fields of earth science. Moreover, since their driving mechanism is still not known in detail, they are also interesting to those who research the motion of liquids in macro scale at a more fundamental level. On the other hand, as they are responsible for the course of a large variety of hydrodynamic driven phenomena at biochemical levels, they are also important from the point of view of environmental science. They also contribute to many water management related issues – like designing the protection zones for water supply inlets, or maintaining the right balance between various tasks that the given reservoir was built for.

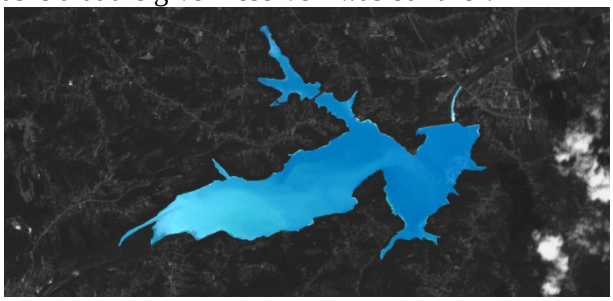

Figure 7. A turbidity current in the Dobczyce reservoir 2019.05.18.

Visible light Sentinel-2 photos may deliver information about the currents in reservoirs as long as the current can be visually distinguished from the surrounding waters. This applies primarily to

turbidity currents (Fig. 7) and eutrophic water currents (Fig. 8). Moreover, in an inverted setup, where clear water enters a turbid or eutrophic area, the resulting current can also be distinguished (Fig. 9).

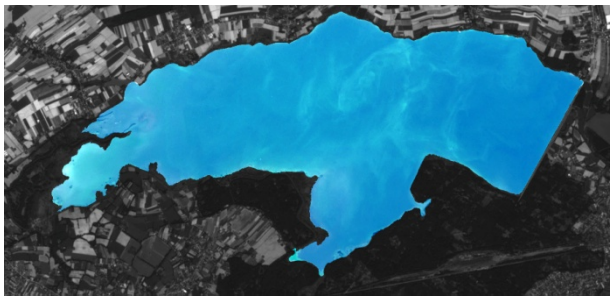

Figure 8. An eutrophic current in the Goczałkowice reservoir.

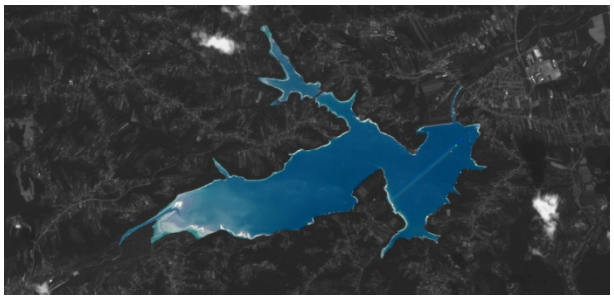

Figure 9. A clear water current entering the Dobczyce reservoir 2018.05.10 (the line visible in the eastern part of the reservoir is a trail of a jet plane).

### 3.3. High discharge turbidity currents

The propagation of high discharge waves through reservoirs is another area of interest in reservoir hydrodynamics where satellite imaging can help, as the turbidity currents induced by high discharge (a.k.a. flooding) conditions can be visible on satellite photos.

Figure 10 contains histograms of the daily measured inflow discharge entering the Dobczyce reservoir along with their average (red line) and mean (blue line) values. Please note that both axes are logarithmic. Panel T ("total") shows the histogram of all the measured values, panel P ("photo") presents the histogram for the values measured only during the days a Sentinel photo has been taken. The four following panels "A" to "D" contain the inflow discharge histograms for the days when appropriately ranked photo has been taken. Comparison of T and P frames leads to the finding that the histograms are similar in shape and their mean values and average values are close to each other as shown in Table 4. On the other hand, the frames dependent on the reservoir visibility differ from one another: as expected, good visibility is coupled with lower discharges and vice versa. Intuitively: rainy weather is associated both with cloudy sky and more water in rivers.

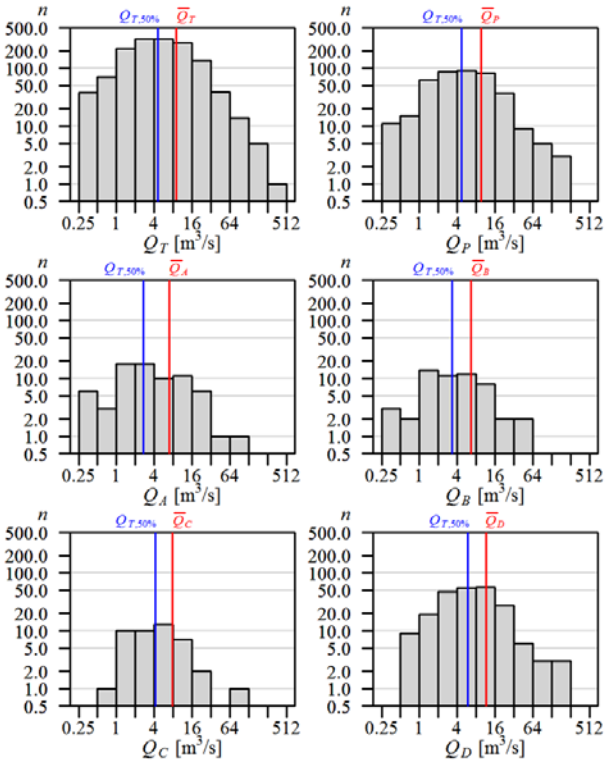


Figure 10. Histograms of the inflow discharge entering the Dobczyce reservoir;
T: all daily values between June 2015 and May 2018;
P: values for the days a Sentinel photo is available;
A: values for the days an A-rated photo is available;
B: values for the days a B-rated photo is available;
C: values for the days a C-rated photo is available;
D: values for the days a D-rated photo is available.

Table 4. High water periods on the Dobczyce reservoir (July 2015 to May 2019).

| | Global | Photo taken | A-rated photo taken | B-rated photo taken | C-rated photo taken | D-rated photo taken |
|---|---|---|---|---|---|---|
| Average Inflow | 9.3 | 10.1 | 7.2 | 6.9 | 7.9 | 12.3 |
| Mean Inflow | 4.8 | 4.9 | 2.9 | 3.5 | 4.2 | 6.3 |

Table 5 presents all the high-water periods that occurred on the Dobczyce reservoir from the beginning of the Sentinel missions until the end of May 2019. In accordance with (Hachaj, 2019), the authors took the daily measured inflow discharge value of 50m$^3$/s as the threshold of "high discharge". As the beginning of a given high discharge event, the day when the discharge reaches 80% of the threshold value (i.e. 40m$^3$/s) was taken; as the end of the event, the day when the discharge falls below 40m$^3$/s was taken. There were 15 high discharge periods

Table 5. High water periods on the Dobczyce reservoir (July 2015 to May 2019).

| No. | High water periods | | Photo | | | |
|---|---|---|---|---|---|---|
| | since | to | A | B | C | D |
| 1 | 22.02.2016 | 24.02.2016 | | | | |
| 2 | 15.05.2016 | 16.05.2016 | | | | |
| 3 | 18.07.2016 | 19.07.2016 | | | | 19.07 |
| 4 | 05.10.2016 | 08.10.2016 | | | | 07.10 |
| 5 | 23.02.2017 | 26.02.2017 | | | | 24.02 |
| 6 | 29.04.2017 | 01.05.2017 | | | | 30.04 |
| 7 | 21.08.2017 | 22.08.2017 | | 21.08 | | |
| 8 | 22.09.2017 | 26.08.2017 | | | | 22.09 |
| 9 | 24.10.2017 | 26.10.2017 | | | | 25.10 |
| 10 | 29.10.2017 | 01.11.2017 | | | 30.10 | 01.11 |
| 11 | 19.07.2018 | 22.07.2018 | 22.07 | | | 19.07 |
| 12 | 23.02.2019 | 24.02.2019 | | | | 24.02 |
| 13 | 29.04.2019 | 02.05.2019 | | | | 30.04 |
| 14 | 15.05.2019 | 18.05.2019 | 18.05 | | | 15.05 |
| 15 | 23.05.2019 | 27.05.2019 | 25.05 | | | 23.05 |
| | | **Total** | **3** | **1** | **1** | **12** |

registered that met the above criteria. They last between 2 and 5 days. It should be mentioned that the events 9 and 10 as well as 14 and 15 were separated by days on which the inflow discharge dropped below $20m^3/s$ and therefore they should be treated as separate events.

There are two main causes of flood discharges – the first being thaw and the second long and/or heavy rainfall. Out of the events presented in Table 5, numbers 1, 5, and 12 are thaw ones, the others were caused by rainfall. The four rightmost columns of the table show the dates the Sentinel photos were taken during the flooding events. Out of the 15 photos taken, 11 show only the cloud cover over the reservoir, two caught some fragments of the reservoir and only 3 (20% of the total number) contain a clear picture of the Dobczyce reservoir. Out of the 5 photos ranked "C" or more, 4 were taken on the last day of the event. This can be explained by the fact that the same clouds that cause the rainfall can also obscure the view of the reservoir. The only exception is event 15, when there was still rainfall present upstream the Raba river, but the sky over the reservoir was clear.

Therefore, the Sentinel-generated material regarding high discharges is still insufficient for detailed analyses. But even now some preliminary comparisons with model predictions can be performed. Figure 11 presents the Dobczyce reservoir taken 2018.07.22. The appropriate values of inflow and outflow discharges on that day were $Q_{in} = 37m^3/s$, $Q_{out} = 62m^3/s$; on the previous day they were $Q_{in} = 83m^3/s$, $Q_{out} = 78m^3/s$ respectively. The wind speed on that day was in range of 1.3m/s with changing directions, which justifies neglecting the wind impact on the water velocity field.

Figure 11. Turbidity current visible on the Dobczyce Lake during a high-water event 2018.07.22.

Figure 12 presents a map of the planar average velocity field calculated by the FESWMS model with adaptive roughness procedure (Hachaj, 2013) applied for the windless weather and inflow and outflow discharges set at $Q_{in} = 40m^3/s$, $Q_{out} = 65m^3/s$. The shape of the simulated main current follows the shape of the real turbidity current quite well. Some additional features like the clockwise loop in the southern bay and the backward current along the northern bank are also reproduced properly in the model. The only noticeable difference is the fact that the turbidity current is not visible close to the dam. In this region, it may get submerged and as such its contrast with the surroundings may be too low to be recognizable, so it is not possible to determine whether it follows the model prediction or not.

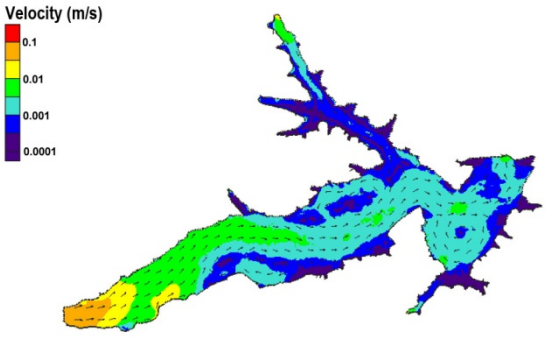


Figure 12. Water velocity map generated with the FESWMS model for the Dobczyce reservoir for the hydrometeorologic conditions as they were 2018.07.22.

To some extent, turbidity and eutrophic currents may be recognized in the photos even when they are not flowing on the surface, but as deep currents, beyond their plunge points, as long as water around is clear and the light penetration at the level of the submerged current is high enough. The issue of submerged currents recognition seems to be a promising field of future research; with a proper calibration, changes in the current colour could possibly be mapped on the depth the current moves at.

### 3.4. Sub-glacial currents

Sentinel-2 visible light images have already been proven to be a good data source regarding ice covering of inland waters (Magnuszewski, 2018). They may also provide some information about sub-glacial flow, as the water currents may be visible through the ice, provided that there is no snow on it. Figure 13 presents a thaw discharge that forms a turbidity current in the Dobczyce reservoir on 2017.02.27 (3 days after high water event 12 shown in Tab 4). That day the reservoir inflow and outflow were: $Q_{in}$ = 11m$^3$/s, $Q_{out}$ = 21m$^3$/s, values that are considered "moderate" for that reservoir, but the turbidity current that formed a few days before, when the inflow exceeded 55m$^3$/s, is still clearly visible, allowing a comparison with results of numerical simulations of sub-glacial water flow. Performing such simulations with a suitable hydrodynamic model is one of the close future plans of the authors.

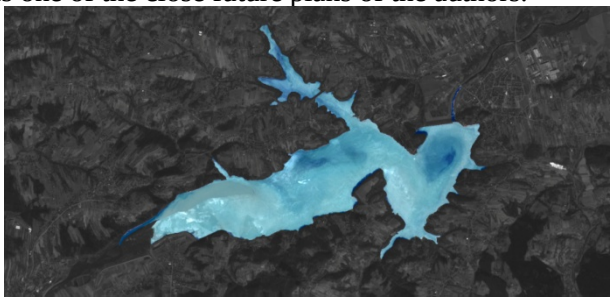

Figure 13. Sub-glacial density current in the Dobczyce reservoir 2017.02.27.

Another example of sub-glacial currents visible is shown in Figure 14. Here the discharge is smaller than it was in the previous case: $Q_{in}$ = 3.7m$^3$/s, $Q_{out}$ = 3.6m$^3$/s. There are meander-like forms visible to the north of the old river bed and embankments that are still present within the reservoir (Fig. 15). This suggests that the flow chooses that part of the reservoir, while water in the southern part remains stagnant. The flower-like radial shape in the northwestern part of the reservoir could possibly be connected with ground water leakages to the reservoir that are known to be present within this water body (Siudy et al., 2006; Trzewik, 2012). As a single image, the photo shown in Figure 14 is difficult to interpret, but it marks a promising direction of future research, as upcoming satellite images to compare it with will appear.

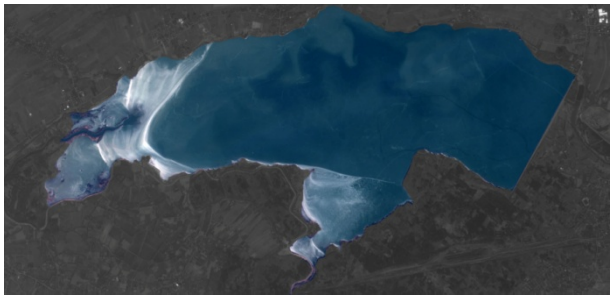

Figure 14. Sub-glacial flow in the Goczałkowice reservoir 2018.03.24.

Figure 15. Bathymetric map of the Goczałkowice reservoir.

### 3.5. Thermal currents

Currently the authors identified two photos that can be interpreted as depicting thermal currents: the first is shown in Figure 16, taken 2017.05.28. The discharge that day was moderately low: inflow $Q_{in}$ = 5.2m$^3$/s, outflow $Q_{out}$ = 7.7m$^3$/s. The wind was mostly eastern (NE to SSE) up to 3 m/s. There were almost no clouds so the solar exposition was high and the temperature that day reached 29$^o$C. The preceding decade was also warm (maximal temperatures 21-29$^o$C) compared to the previous one (maximal temperatures 14-26$^o$C). This allows to set a hypothesis that the disturbances visible in the photo, especially ones in the deep, eastern part of the reservoir, are of thermal nature.

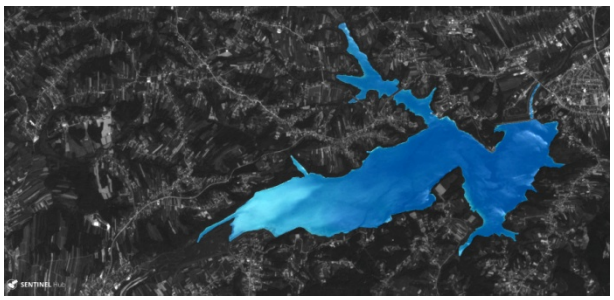

Figure 16. Suspected thermal currents visible on the Dobczyce reservoir 2017.05.28.

The second photo containing suspected thermal currents has been taken 2019.06.12 and it shows the Goczałkowice reservoir (Fig. 17). The discharge that day was low: $Q_{in}$ = 1.6m$^3$/s, outflow $Q_{out}$ = 3.6m$^3$/s. The wind speed was up to 4m/s, and its direction was changing from ENE to SSW. As in the previous case the sky was almost clear and the maximal temperature reached 30ºC. During the preceding week the daily maximal temperature was growing each day after a previous relatively cold period of maximal temperatures lower than 20ºC. In the photo it can be seen that most of the observed currents start perpendicularly to the southern shallow banks; their propagation from shallow southern shore towards the deeper parts of reservoir generally follow the slope of the reservoir bed (Fig. 17). This backs the hypothesis that gravity and density differences of thermal origin are the driving forces there, rather than wind.

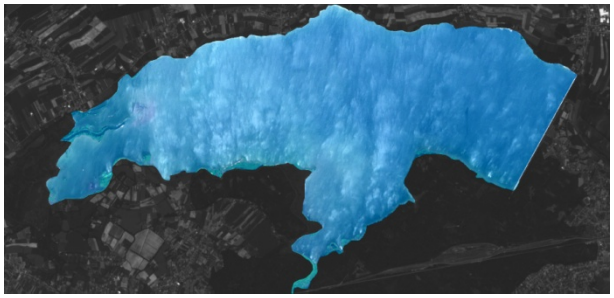

Figure 17. Suspected thermal currents visible on the Goczałkowice reservoir 2019.06.12.

## 4. CONCLUSIONS

Satellite visible light photography can be a source of data regarding hydrodynamic phenomena that occur in storage reservoirs. The Sentinel-2 satellites provide 10m resolution images once or twice every five days, depending on the object's location. However, in Central Europe, cloudy weather causes a substantial percentage of images to be unfit for analysis. In the Polish Carpathian region one can expect that only up to about 1/5 of the photographs will show the whole reservoir without any obscuring clouds or mists. If some minor obscuring is acceptable, the fraction of the images that can be considered "good" increases up to about 1/3. The expected visibility varies throughout the year, following the expected clear sky percentage for a given period. In the Polish Carpathians, the best visibility occurs in August, while the worst in December. Due to the fact that both the discharge in a reservoir and its visibility depend on weather, one should expect lower mean and average discharges for the days "clear" or "good" photos are taken.

The features that give an insight into the reservoir hydrodynamics that are visible on satellite photos are density currents. They can be:

• Turbidity currents that occur during and shortly after high discharge periods.

• Clear (a.k.a. reverse turbidity) currents, when clear water enters a still turbid reservoir; such currents occur at the end of high discharge periods.

• Eutrophic currents that appear after a warm period when eutrophicated water is carried out of the eutrophication zones.

• Thermal convection currents that appear in reservoirs late spring and mid-autumn. (However, the authors found only images containing suspected spring thermal currents in the photos of the Upper Vistula catchment reservoirs.)

• Sub-glacial turbidity currents occurring during thaws.

The shapes and sizes of visible currents may provide an additional mean to calibrate and validate numerical models of reservoir hydrodynamics (like the authors used the photo of the Dobczyce reservoir to validate the predictions of the FESWMS model).

Among the directions of future research regarding the Sentinel-2 photos of the Polish Carpathian reservoirs the authors would like to point out:

• Checking the possibility of density currents identification in non-visible electromagnetic bands captured by Sentinel-2.

• Development and implementation of an algorithm of current recognition, at least for the "clear", A-rated photos.

• Calibration of a sub-glacial flow numerical model using the Sentinel-2 images.

Since the Sentinel-2 satellites are fully operational now, the number of photos in the ESA database is expected to continuously increase, yielding more and more data for further analyses.

## REFERENCES

**Abbasi, A., Annor, F. & Van de Giesen, N.,** 2016. *Investigation of Temperature Dynamics in Small and Shallow Reservoirs, Case Study: Lake Binaba*. Upper

East Region of Ghana, Water, (8(3)).

**Akiyama, J. & Stefan, H. G.,** 1984. *Plunging Flow into a Reservoir: Theory*. Journal of Hydraulic Engineering, (110(4)), 484–499.

**Augustyn, L.,** 2010. *The influence of the Czorsztyn-Niedzica and Sromowce Wyżne hydroelectric power station on the ichthyofaunal of the Dunajec River in the Pieniny region.* Monografie Pienińskie, 2, 227-239

**Bartoszek, L. & Czech, D.,** 2014. *The susceptibility of the Solina dam reservoir to degradation.* Journal of Civil Engineering, Environment and Architecture, t. XXXI, z. 61 (4/14), 35-53 [in Polish].

**Bielak, B.,** 2009. *Variability in tourist traffic in the vicinity of reservoirs in the Polish Carpathian Mountains.* Prace Geograficzne, 121, 25-37 [in Polish].

**Bogdał, A., Kowalik, T.& Witoszek, K.,** 2015. *Effect of the Goczałkowice reservoir on the changes of water quality in the Vistula river.* Ecological Engineering, 45, 124-134 [in Polish].

**Chen, G. & Fang, X.,** 2015. *Sensitivity Analysis of Flow and Temperature Distributions of Density Currents in a River-Reservoir System under Upstream Releases with Different Durations.* Water, (7), 6244–6268.

**Condé, R. de C., Martinez, J. M., Pessotto, M. A., Villar, R., Cochonneau, G., Henry, R., Lopes, W. & Nogueira, M.,** 2019. *Indirect Assessment of Sedimentation in Hydropower Dams Using MODIS Remote Sensing Images.* Remote Sensing, 11(3), 314.

**Copernicus,** 2019. *https://www.copernicus.eu*. European Union Copernicus Program.

**Cortés, A., Fleenor, W. E., Wells, M. G., De Vicente, I. $ Rueda, F. J.,** 2014. *Pathways of river water to the surface layers of stratified reservoirs.* Limnology and Oceanography, 59(1), 233–250.

**Dai, A. & Garcia, M. H.,** 2009. *Analysis of plunging phenomena.* Journal of Hydraulic Research, 47:5, 638-642.

**De Cesare, G., Schleiss, A. & Hermann, F.,** 2001. *Impact of turbidity currents on reservoir sedimentation*. J. of Hydraulic Engineering, Vol. 127, Issue 1, 6-16.

**Dörnhöfer, K. & Oppelt, N.,** 2016. *Remote sensing for lake research and monitoring - Recent advances.* Ecological Indicators, 64, 105–122.

**EO Browser,** 2019. https://apps.sentinel-hub.com/eo-browser/

**European Space Agency,** 2019. *https://www.esa.int/ESA, https://sentinel.esa.int*

**Ford, D. E.,** 1990. *Reservoir transport processes*. In: **Thornton, K. W., Kimmel, B. L., & E., P. F. [eds]** *Reservoir Limnology*. New York: John Wiley & Sons, Inc., 15–42.

**Froehlich, D. C.,** 2003. *User's Manual for FESWMS FST2DH.* 2002 (October), 1–209.

**Gatti, A. & Bertolini, A.,** 2015. *Sentinel-2 Products Specification Document.* Thales Alenia Space.

**Gatti, A. & Galoppo, A.,** 2018. *Sentinel-2 Products Specification Document.* Thales Alenia Space.

**Goleij, H., Haghiabi, A. H. & Parsaie, A.,** 2017. *An experimental study on plunging depth of density currents.* Frontiers of Structural and Civil Engineering, 11(4), 388–395.

**González-Jorge, H., González-deSantos, L. M., Martínez-Sánchez, J., Sánchez-Rodríguez, A. & Lorenzo, H.,** 2018. *Automatic Measurement of Water Height in the As Conchas (Spain) Reservoir Using Sentinel 2 and Aerial LiDAR Data.* Remote Sensing, 10(6), 902.

**GUS,** 2017. *Rocznik Statistical Yearbook of Agriculture 2017.* Dział Wydawnictw Statystycznych GUS.

**Hachaj, P. S.,** 2007. *Modelling of water velocity field in Dobczyce reservoir – calculation grid and preliminary results.* Czasopismo Techniczne, Z. 2-Ś/2007, 99-111[in Polish].

**Hachaj, P. S.,** 2013. *The 'River Memory' Effect: An Attempt to Understand and Model it.* GeoPlanet: Earth and Planetary Sciences, 315-326.

**Hachaj, P. S.,** 2019. *Analysis of dammed reservoir hydrodynamics for water management purposes: the model and its use cases.* Wydawnictwo Politechniki Krakowskiej [in Polish].

**Hachaj, P. S., Szlapa, M. & Tutro, M.,** 2014. *Modeling of water dynamics in retention reservoirs - case study*. Saarbrücken: LAP Lambert Academic Publishing.

**He, Z., Zhao, L., Hu, P., Yu, C. & Lin, Y. T.,** 2018. *Investigations of dynamic behaviors of lock-exchange turbidity currents down a slope based on direct numerical simulation.* Advances in Water Resources. Elsevier Ltd, 119(September 2017), 164–177.

**Hennig, J. & Hennig, A.,** 1991. *Zbiorniki retencyjne.* In: **Dynowska, I. & Maciejewski, M. [eds]:** *Dorzecze górnej Wisły. Część II.* PWN, 121-143 [in Polish].

**Hu, P., Pähtz, T. & He, Z.,** 2015. *Is it appropriate to model turbidity currents with the three-equation model?*. Journal of Geophysical Research F: Earth Surface. Blackwell Publishing Ltd, 120(7), 1153–1170.

**Jachniak, E. & Suchanek, I.,** 2015. *The eutrophication of the Tresna dam reservoir in terms of its recreational use.* Ecological Engineering, 44, 170-177 [in Polish].

**Jaguś, A. & Rzętała, M.,** 2010. *The Czorsztyn and Sromowce Reservoirs – location, characteristics and nomenclature.* Monografie Pienińskie, 2, 9-22 [in Polish].

**Jokiel, P., Marszelewski, W. & Pociask-Karteczka, J.,** 2017. *Hydrology of Poland.* Wydawnictwo Naukowe PWN SA [in Polish].

**Karaoui, I., Arioua, A., Boudhar, A., Hssaisoune, M., El Mouatassime, S., Ait Ouhamchich, K., Elhamdouni D., El Amrani Idrissi, A., & Nouaim, W.,** 2019. *Evaluating the potential of Sentinel-2 satellite images for water quality characterization of artificial reservoirs: The Bin El Ouidane Reservoir case study (Morocco).* Meteorology Hydrology and Water Management, 7(1).

**Karasiak, N., Sheeren, D., Fauvel, M., Willm, J., Dejoux, J. F., Monteil, C.,** 2017. *Mapping tree species of forest in southwest France using Sentinel-2 image time series.* In: 2017 9th International workshop on the Analysis of Multitemporal Remote Sensing Images (MultiTemp), 1-4.

**Koszelnik, P.,** 2013. *The Role of Silicon in the Process of Eutrophication of the Waters – Solina and Myczkowce Reservoirs Case Study*. Annual Set The Environment Protection, 15, 2218-2231 [in Polish].

**Lacroix, P., Bièvre, G., Pathier, E., Kniess, U. & Jongmans, D.,** 2018. *Use of Sentinel-2 images for the detection of precursory motions before landslide failures.* Remote Sensing of Environment, 215 (2018), 507-516.

**Lavrova, O.Y., Soloviev, D.M., Strochkov, M.A., Bocharova, T.Y. & Kashnitsky, A.V.,** 2016. *River plumes investigation using Sentinel-2A MSI and Landsat-8 OLI data.* Remote Sens. Ocean. Sea Ice, Coast. Waters, Large Water Reg.

**Liu, H., Li, Q., Shi, T., Hu, S., Wu, G. & Zhou, Q.,** 2017. *Application of Sentinel 2 MSI images to retrieve suspended particulate matter concentrations in Poyang Lake.* Remote Sensing 9, 761.

**Magnuszewski, A.,** 2018. *Application of satellite Sentinel-1 radar images for description of ice phenomena on Dębe reservoir.* Acta Sci. Pol., Formatio Circumiectus, 17 (4), 121–130.

**Majewski, W.,** 2013. *General characteristics of the Vistula and its basin.* Acta Energetica, 2/15, 6-15.

**Meiburg, E. & Kneller, B.,** 2010. *Turbidity Currents and Their Deposits.* Annual Review of Fluid Mechanics, 42(1), 135-156.

**MSI Instrument,** 2019. *MSI Instrument – Sentinel-2 MSI Technical Guide*. https://earth.esa.int/web/sentinel/technical-guides/sentinel-2-msi/msi-instrument

**Neverova-Dziopak, E. & Droździk, A.,** 2017. *Comparative Analysis of Physico-Chemical and Trophic Water State of Czaniec and Goczalkowice Dam Reservoirs in the Period of 2011–2015.* Ochrona Srodowiska, 39, No. 2, 11–16 [in Polish].

**Pahlevan, N., Chittimalli, S. K., Balasubramanian, S. V. & Vellucci, V.,** 2019. *Sentinel-2/Landsat-8 product consistency and implications for monitoring aquatic systems.* Remote Sensing of Environment, 220 (October 2017), 19-29.

**Palmer, S.C.J., Kutser, T. & Hunter, P.D.,** 2015. *Remote sensing of inland waters: Challenges, progress and future directions.* Remote Sensing of Environment, 157, 1–8.

**Rapinel, S., Mony, C., Lecoq, L., Clément, B., Thomas, A. & Hubert-Moy, L.,** 2019. *Evaluation of Sentinel-2 time-series for mapping floodplain grassland plant communities.* Remote Sensing of Environment, 223(2019), 115-129.

**Robak, A., Gadawska, A., Milczarek, M. & Lewiński, S.,** 2016. *The detection of water on Sentinel-2 imagery based on water indices.* Teledetekcja Środowiska, 55 (2016/2), 59–72 [in Polish].

**Savage, S. B. & Brimberg, J.,** 1975. *Analysis Of Plunging Phenomena In Water Reservoirs.* Journal of Hydraulic Research, 13(2), 187–205.

**Schleiss, A. J., Althaus, J. M. I. J.; De Cesare, G. & Boillat, J. l.,** 2009. *Turbidity currents at the origin of reservoir sedimentation, case studies.* In: The 23rd Congress of the Int. Commission on Large Dams CIGB-ICOLD, 58–60.

**Silva, T. S. F., Costa, M. P. F., Melack, J. M. & Novo, E. M. L. M.,** 2008. *Remote sensing of aquatic vegetation: theory and applications.* Environmental Monitoring and Assessment, 140, 131 – 145.

**Siudy, A.,** 2006. *Wielofunkcyjny zbiornik retencyjny Goczałkowice na Małej Wiśle i jego znaczenie dla gospodarki wodnej Górnego Śląska.* In: **Więzik, B. [eds]:** *50-lecie budowy zbiornika wodnego na Małej Wiśle w Goczałkowicach*. Materiały Konferencji Naukowo-Technicznej, Górnośląskie Przedsiębiorstwo Wodociągów Spółka Akcyjna, Katowice, 7-22 [in Polish].

**Sojka, M., Jaskuła, J., Wróżyński, R. & Waligórski, B.,** 2019. *Application of Sentinel-2 satellite imagery to assessment of spatio-temporal changes in the reservoir overgrowth process – a case study: Przebędowo, west Poland.* Carpathian Journal of Earth and Environmental Sciences, 14(1), 39-50.

**Thornton, J., Steel, A. & Rast, W.,** 1996. *Reservoirs* In: **Chapman, D. [eds]** *Water Quality Assessments - A Guide to Use of Biota, Sediments and Water in Environmental Monitoring*. 2nd edn. Cambridge: UNESCO/WHO/UNEP, p. 41.

**Trzewik, M.,** 2012. *Glacial phenomena in the Goczałkowice reservoir,* Politechnika Krakowska, MSc Thesis [in Polish].

**Vanino, S., Nino, P., De Michele, C., Falanga Bolognesi, S., D'Urso, G., Di Bene, C., Pennelli, B., Vuolo, F., Farina, R., Pulighe, G. & Napoli, R.,** 2018. *Capability of Sentinel-2 data for estimating maximum evapotranspiration and irrigation requirements for tomato crop in Central Italy.* Remote Sensing of Environment, 215, 452–470.

**Williams, S., Petersen, M., Bremer, P. T., Hecht, M., Pascucci, V., Ahrens, J., Hlawitschka, M. & Hamann, B.,** 2011. *Adaptive extraction and quantification of geophysical vortices.* IEEE Transactions on Visualization and Computer Graphics, 17(12), 2088–2095.

**Woś, A.,** 1996. *Owerview of the polish climate*, Wydawnictwo Naukowe UAM [in Polish].

Received at: 14. 12. 2019
Revised at: 26. 01. 2020

Accepted for publication at: 10. 02. 2020
Published online at: 27. 02. 2020